

Combined Individual Pitch and Flap Control for Load Reduction of Wind Turbines

Antje Dittmer¹, Bernhard Osterwinter², Daniel Ossmann²

¹ German Aerospace Center (DLR), Institute of Flight Systems, Lilienthalplatz 7, 38108 Brunswick, Germany

² Munich University of Applied Sciences HM, Department of Mechanical, Automotive and Aeronautical Engineering, Lothstr. 64, 80335 Munich, Germany

E-mail: antje.dittmer@dlr.de, daniel.ossmann@hm.edu

Abstract. In this paper individual pitch control is combined with trailing-edge flap (TEF) control, both designed as multi-loop proportional-integral-derivative (PID) controllers, to significantly reduce blade damage equivalent loads. OpenFAST NREL 5MW aerodynamics are enhanced with dedicated aerodynamic polars of TEF blade elements. The NREL 5MW model, including the TEF extension, is incorporated into Simulink, and PID controller parameters are optimized in a closed-loop optimization setup. The DEL decrease is confirmed via an extensive simulation campaign using the non-linear wind turbine simulation environment.

1. Introduction

Active aerodynamic load control (AALC) of wind turbines has been a very active area of research in the last two decades, as turbine size and damage equivalent loads (DEL) acting on blades and towers increase. Individual pitch control (IPC) has been applied in various studies to enable blade root moment reduction: Promising simulation results exist with different control algorithms e.g. proportional-integral-derivative (PID) [1], linear quadratic Gaussian (LQG) [2], and model predictive (MPC) control [3]. Field tests confirm the potential of IPC, see [4] and [5]. Recently, trailing-edge flaps (TEF) for wind turbines have been suggested for blade root load reductions in [6] and [7]. As TEF add an additional degree of freedom to the wind turbines' actuation, there are also studies combining the two methods: In [8], the standard deviation of blade root flapwise bending moments is reduced up to 32% for two wind test cases with turbulence class A, at 16 m/s and 20 m/s mean wind speed. Turbulence class A at 18 m/s mean wind speed is used in [9] to investigate the trade-off between load reduction and actuator activity. In [10], the blade root flapwise moments and blade tip out-of-plane deflection are both reduced by over 50%, while also decreasing tower moments for a wind test case of turbulence class B at 20 m/s. This work, summarizing results from [11], extends the scope of previous solutions by optimizing the combined individual pitch and trailing-edge control strategy for the whole region III operation of a wind turbine by incorporating nine different wind speeds, ranging from 12 m/s to 25 m/s for turbulence class A. We confirm that AALC does not reduce power output - i.e., the same power is obtained at reduced DEL. The required additional actuator power due to IPC is investigated, as in [9]. We generate a sufficient number of verification wind data sets, nine for turbulence class A, each with a different seed, and nine for turbulence class B, to confirm the applicability of our AALC design.

2. Simulation Model

The National Renewable Energy Laboratory’s (NREL) OpenFAST simulation software [12] is used to investigate the benefits of combining individual pitch and trailing-edge flap control. The NREL 5MW wind turbine model, see [13] for the documentation of the simulation model, is modified to implement controllable trailing-edge flaps on the rotor blades. The original NREL 5MW model without TEF serves as a reference for analyzing the aerodynamic effects of these modifications on the simulated operation of the turbine. The NREL 5MW is a variable-speed, variable-pitch controlled, upwind turbine with a hub height of 90 m and a rotor diameter of 126 m. It has a cut-in wind speed of 3 m/s, a rated wind speed of 11.4 m/s, and a cut-out wind speed of 25 m/s. This section describes the rotor blade layout and the TEF design, including their integration into the NREL 5MW model. An overview of the baseline power controller as well as a description of open-loop verification simulation are also provided.

2.1. Rotor Blade Geometry and Aerodynamics

The rotor blades of the NREL 5MW turbine are defined by eight distinct cross-sectional profiles distributed along the blade length, as illustrated in Figure 1, and comprise 19 nodes, each with specific geometric profile shapes. At the root, cylindrical profiles connect to the rotor hub, accommodating high bending moments and pitch adjustments. The profiles transition from the DU series, developed at Delft University of Technology, near the root to the NACA64 profile in the outer 29% of the blade, characterized by decreasing thickness towards the tip. The blade section with trailing-edge flaps, which cover the whole NACA64 blade section, is marked in red. The flap-to-blade chord ratio amounts to 20%. The aerodynamic model of the blade enhanced with TEF requires input data on lift, drag, and pitching moment coefficients for all profiles across various blade angles of attack and a variety of flap deflection angles. The three main factors influencing these aerodynamic properties are surface roughness, Mach number, and Reynolds numbers. The OpenFAST neglects surface roughness variations due to contaminants. The airflow is assumed to be incompressible with a Mach number of 0.25 at the blade tip. Interpolating between different polars is implemented in OpenFAST based on a user-defined parameter, by default the Reynolds number. In this work the interpolation between polars is performed based on the flap positions. As only one interpolation parameter can be defined, the Reynolds number distribution depicted in Figure 1 is used for all wind speeds. Care was taken to model the distribution of Reynolds numbers along the rotor blade at this wind speed as realistically as possible. Realistic Reynolds numbers for rotor blades range from one to eight million are obtained from an OpenFAST Simulation with turbulence class A at a mean wind speed of 12 m/s. The resulting Reynolds number distribution is depicted in Figure 1. The OpenFAST aerodynamic models of the rotor blades are extended with additional airfoil polars based on this distribution.

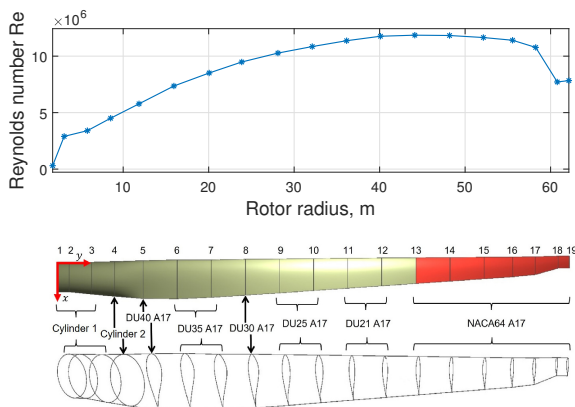


Figure 1. Span-wise distribution of Reynolds numbers Re at wind speed $V = 12$ m/s (from OpenFAST simulation) and blade geometry with cylinder, DU40, DU35, DU30, DU25, DU21 and NACA64 profiles with TEF location covering the NACA64 section marked in red.

2.2. Polar Calculation with xflr5 and XFOIL

The aerodynamic coefficients of rotor blade profiles for the TEF enhanced blades are calculated using the programs xflr5 and XFOIL, see [14]. XFOIL uses a higher-order panel method to analyze and design airfoil profiles, incorporating variables like Reynolds number, Mach number, and a transition criterion for calculating the shift from laminar to turbulent flow. The turbulence degree of the incoming flow determines the appropriate transition criterion value, with the default value set at 9, approximating a median turbulence level as per XFOIL’s documentation. For fluid properties, standard sea-level values from the International Standard Atmosphere (ISA) are used. The aerodynamic coefficients for the respective profiles are calculated based on the Reynolds numbers selected from Figure 1. The coefficients generated by xflr5 and XFOIL are not directly suitable for wind turbine simulation as AeroDyn15 requires coefficients over an angle of attack range from -180° to $+180^\circ$. Since XFOIL’s panel methods yield accurate results only up to the point of flow separation, the polars are extrapolated to cover the entire required angle range. This extrapolation is performed using the AirfoilPrep preprocessor developed by NREL, applying the Viterna method for extrapolating polars, see for details e.g. [15]. Additionally, corrections are made to account for three-dimensional flow effects caused by the rotor blade’s rotation. Factors like Coriolis and centrifugal forces increase the maximum lift coefficients in the inner rotor areas. These 3D effects are corrected using functions integrated into AirfoilPrep. Figures 2 and 3 illustrate the extrapolated and corrected lift and drag coefficients over the angle of attack for rotor blade profiles with different flap angles. Figure 2 shows that a positive flap deflection, i.e. the flap moves backwards with respect to the chord line of the local blade profile with an undeflected flap, leads to an increase in lift coefficients c_l and hence in lift. The point of maximum lift coefficient shifts to a smaller angle of attack than with a neutral flap position. A negative flap deflection has the opposite effect. The lift coefficients are reduced and the point of maximum lift coefficient shifts to higher angles of attack. This corresponds to the expected effects of different trailing-edge flap deflections on the lift. Figure 3 visualizes the drag coefficient. The curves of the drag coefficient c_d appear smooth and physically meaningful for angles of attacks above -27° . Note that there is a sudden reversal of the vertical staggering of the polars below this value. There is neither a physical explanation for this effect, nor is any discontinuity observed for the rotor profile without trailing-edge flap. It can be assumed that the extrapolation method does not work optimally for profiles with flaps at these high TEF angles that would lead to flow separation and stall. However, this can be disregarded as the range of TEF angles of attack in the simulations in the outer area of the rotor blades do not exceed -27° during normal operation. As this study uses OpenFAST v3.2.1, no additional code needs to be added for the TEF inclusion, unlike in previous studies that leveraged previous versions of FAST. The obtained coefficients are summarized in a text file, which is included as a parameter in the Airfoil Information section of the AeroDyn15.dat file of the NREL 5MW model.

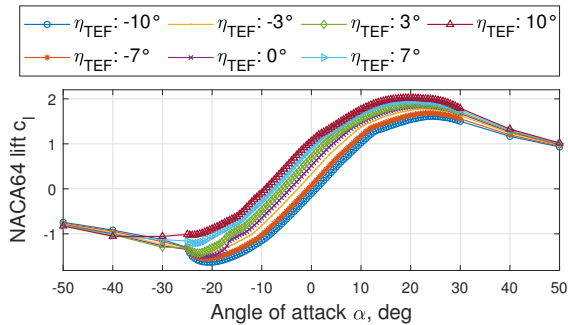


Figure 2. Lift coefficient c_l at different TEF angles.

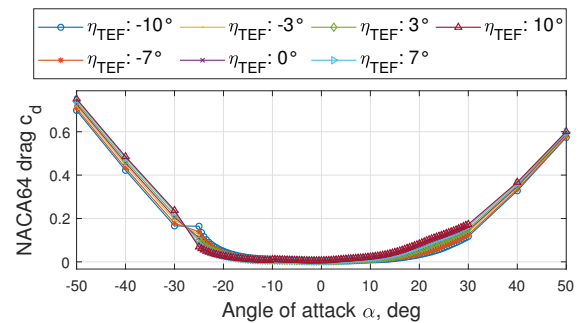


Figure 3. Drag coefficient c_d at different TEF angles.

2.3. Baseline Power Controller

In order to realistically simulate a modern turbine, a control system controlling rotor speed and generator torque is required. Such a control system ensures the maximum power output at each wind speed, controlling the generator torque M_{gen} and blade pitch angle β . Therefore, generator torque is used for maximizing power yield at wind speeds above the cut-in wind speed and below the rated speed of a turbine, called region II. The blade pitch is used to keep power output constant at rated power for wind speeds above rated wind speed and below cut-out wind speed, i.e., wind speeds in region III. The aim is to further decrease these mechanical loads by the AALC. Note that this load reduction controller using IPC together with TEF-control is an add-on controller to the baseline control system. This is possible as cyclic pitch motions are induced, which are effectively decoupled from the collective pitch motion ensuring the maximum power output above rated wind speed. The baseline controller is the power controller available within Delft University of Technology's FASTTool, see [16]. FASTTool features a MATLAB graphical user interface for setting up simulations and tuning control parameters for an underlying Simulink model, representing the dynamics of the NREL 5MW turbine. The OpenFAST NREL 5MW model, including the TEF model described above, is integrated with an S-Function into the Simulink model. In our study, the Simulink block for the power controller from FASTTool is used without any changes. Nevertheless, a short overview of the controller is given here for completeness: The power controller receives feedback in the form of generator rotational speed, ω_{gen} . In regions I 1/2 and II, the $k\omega^2$ control law is used for the generator torque based on a tabulated function of ω_{gen} . In region I 1/2, the start-up region just below the cut-in wind speed, a multiplication factor is applied to calculate the reference generator torque $M_{\text{gen,ref}}$. In region II an optimal factor K^* is multiplied to the square of the rotational speed. A smooth linear interpolation is used in region II 1/2 up to rated rotational speed. In region III, the collective pitch control strategy is based on a scheduled proportional-integral controller. The two gains are scheduled with the generator speed, i.e., $K_P(\omega_{\text{gen}})$ and $K_I(\omega_{\text{gen}})$. This dynamic gain adjustment helps to efficiently track the maximum rotor speed. The gain values for this collective pitch control are left unchanged from the original FASTTool repository.

2.4. Verification of Simulation Model

The modified NREL 5MW turbine model presented in the previous section is tested in open-loop simulations with regard to the plausibility of the influence of the TEF position on the simulation results. The aerodynamic model of the trailing-edge flap is included. Open-loop control inputs of the TEF deflection angle η are analyzed in order to investigate its suitability with regard to the desired DEL reduction. The effects of flap deflections on different parameters relevant to the operational quality of the wind turbine, such as forces and moments as well as power yield, are investigated. Figure 4 shows a block diagram to illustrate the control structure used for these verification tests, with seven control inputs and the wind of the selected test case V_{TC} as a disturbance. The actuators for the pitch angle adjustment of the rotor blades are modeled as first order transfer function with position and rate limitations. The influences of different TEF positions for steady-state operating conditions are discussed in section 6.

3. Controller Design

The main design objective of the presented Active Aerodynamic Load Control (AALC) controller, consisting of the combination of IPC and the individual control of the flaps (IFC), is the reduction of structural moments, focusing on flapwise blade root bending moments. The overall controller layout is shown in Figure 5. The baseline controller, depicted in Figure 4, is enhanced with IPC, with the individual pitch demand added to the collective pitch reference, as well as IFC which changes the TEF position. All six AALC control output signals are calculated via Multiblade Coordinate Transformation (MBC), based on the three flapwise blade

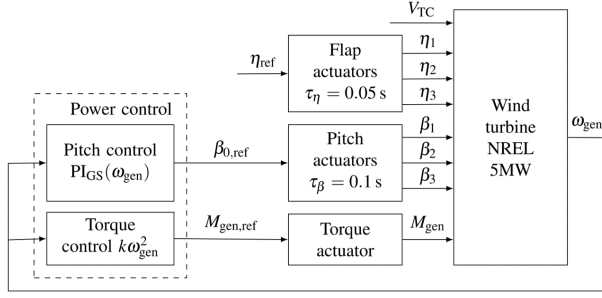


Figure 4. Block diagram for open-loop verification with baseline power control in closed loop and open-loop collective TEF control inputs.

root moments, M_{yb1} , M_{yb2} , and M_{yb3} , as well as the rotor azimuth Ψ . This section first reviews MBC and the allocation of IPC and IFC signals then discusses the design of these controllers.

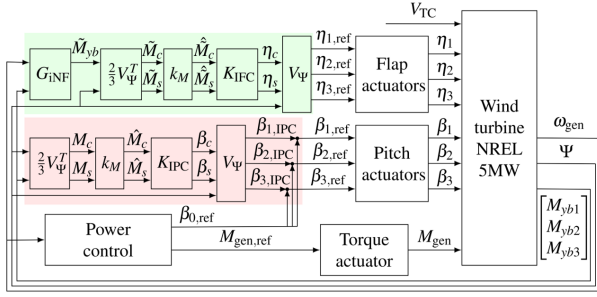


Figure 5. Block diagram for closed-loop verification testing with baseline power control, individual pitch and TEF closed loop control.

3.1. Multiblade Coordinate Transformation and Control Allocation

MBC enables the conversion of dynamic loads from the rotating blade coordinate system, defined by the azimuth angle Ψ , to a fixed tower coordinate system. Specifically, load components in the 1P frequency range are transformed via the MBC to quasi-static loads. Hence, MBC allows for a more accurate assessment of the loads acting on the turbine tower and other non-rotating components. Applying MBC to convert the rotating blade root flap moments into a fixed coordinate system for a three-bladed wind turbine results in the matrix calculation

$$\begin{bmatrix} M_c \\ M_s \end{bmatrix} = \frac{2}{3} \begin{bmatrix} \cos(\Psi) & \cos(\Psi + \frac{2\pi}{3}) & \cos(\Psi + \frac{4\pi}{3}) \\ \sin(\Psi) & \sin(\Psi + \frac{2\pi}{3}) & \sin(\Psi + \frac{4\pi}{3}) \end{bmatrix} [M_{yb1}, M_{yb2}, M_{yb3}]^T \quad (1)$$

with M_{ybi} as the flapwise blade root moment of the i^{th} blade as inputs, and the blade tilt moment M_c and yaw moment M_s in the non-rotating system as outputs. The moments M_c and M_s are used to calculate two cyclic control signals q_c and q_s , i.e., β_c and β_s for IPC, and η_c and η_s for IFC. The control signal q_i of the i^{th} blade is calculated via the inverse MBC transformation

$$\begin{bmatrix} q_1 \\ q_2 \\ q_3 \end{bmatrix} = \underbrace{\begin{bmatrix} \cos(\Psi) & \sin(\Psi) \\ \cos(\Psi + \frac{2\pi}{3}) & \sin(\Psi + \frac{2\pi}{3}) \\ \cos(\Psi + \frac{4\pi}{3}) & \sin(\Psi + \frac{4\pi}{3}) \end{bmatrix}}_{V_\Psi} \begin{bmatrix} q_c \\ q_s \end{bmatrix}, \quad (2)$$

where the signal q_i denotes $\beta_{i,IPC}$ and $\eta_{i,ref}$ in IPC and IFC, for the i^{th} blade or flap, respectively. Note that the transpose of the matrix V_Ψ from equation (2), multiplied by $2/3$, is equal to the MBC matrix from equation (1), see also [17]. In the context of this study, and as is common in related literature, see e.g. [10], the tilt and yaw moments M_c and M_s are controlled via q_c and q_s independently, i.e., any remaining coupling following the MBC transformation between q_c and

M_s as well as q_s and M_c is neglected. As the wind turbine dynamics can be modeled as a linear time-invariant (LTI) system after transforming rotor blade dynamics into a fixed coordinate system, using MBC from equation (1), a simple, intuitive control approach is adopted. Four separate Single-Input-Single-Output (SISO) controllers, two for IPC and IFC, respectively, are designed to reduce the transformed moments M_c and M_s . The system is now over-actuated, i.e., two moments, M_c and M_s , need to be mitigated, but four control inputs, η_c , η_s , β_c , and β_s , are available. This offers the possibility of a frequency separation as a form of Control Allocation (CA). To achieve this frequency separation of individual pitch control and individual flap control inverse notch filters are implemented in the AALC controller. The 1P loads in the frequency spectrum of the blade root bending moments are addressed with the IPC control loop. The 2P loads are addressed with the trailing-edge flap controller making use of the fast flap dynamics. While modern Multiple-Input-Multiple-Output (MIMO) controllers, e.g., AALC extension of our H_∞ control [4, 17] or MPC [18], have the potential to optimize the available control inputs regarding the criteria listed in section 4 more efficiently, this simple, intuitive CA is selected as the resulting controller does not employ an observer based structure and thus avoids the explicit integration of a mathematical plant model.

3.2. Individual Pitch Control for 1P Load Reduction

The IPC controller K_{IPC} , illustrated in the red part of Figure 5, receives the blade root flap moments M_{yb1} , M_{yb2} , and M_{yb3} from the rotating coordinate systems, transforming them into fixed coordinate system moments M_c and M_s via MBC without additional filtering. This approach obviates the need for low-pass filtering within the IPC loops, as the actuator models already provide inherent low-pass filtering characteristics. The transformed moments are scaled with $k_M = 10^{-5}$, and \hat{M}_s and \hat{M}_c are passed to two identical SISO controllers. These controllers are based on the assumption that the transformed moments become largely independent after the transformation. The LTI nature of the transformed system allows for the potential use of PID controllers. Moreover, for IPC, which focuses on mitigating low-frequency load changes, particularly the 1P loads caused by tower wake effects and wind speed variations, a controller with an integral gain is first tuned manually. The integral component adequately addresses the control requirements by minimizing the steady-state error of the transformed moments and thus effectively targets the minimization of the 1P loads in the rotating coordinate system. This aids in decoupling of the IPC from the IFC controller, with the IFC used for controlling higher frequencies. The calculated control signals β_c and β_s are converted back to the rotating blade coordinate systems via the inverse MBC given in equation (2), resulting in the three signals $\beta_{i,IPC}$. The IPC exclusively calculates individual pitch angle components, avoiding interference with collective pitch angles calculated by the baseline power controller. The pitch angle commands, passed to the pitch actuators, $\beta_{i,ref}$ are calculated by adding the collective pitch angle command $\beta_{0,ref}$ to these individual pitch reference signals. The actuator model is implemented as a first order transfer function with time constant $\tau_\beta = 0.1$ with the angle limited from -2° to 90° and the rate limited from $-8^\circ/s$ to $8^\circ/s$. The pitch actuator angles β_i are then applied to the OpenFAST NREL 5MW wind turbine model.

3.3. Trailing-edge Flap Control and Inverse Notch Filter for 2P Load Reduction

The PID controller for the individual trailing-edge flap control K_{IFC} is constructed similarly to the IPC, with the MBC and inverse MBC forming central elements, encompassing the two identical SISO controllers for controlling the transformed moments. A key difference is that the blade root flap moment signals are filtered through an inverse notch filter before MBC processing, amplifying selected frequencies

$$G_{iNF}(s) = (s^2 + 2kDfs + f^2)/(s^2 + 2kDfs + f^2), \quad k = 10, \quad D = 0.1$$

with frequency f set as twice the value of the current rotor frequency f_{rot} and s being the Laplace variable. This enhances 2P load amplitudes in the signals, enabling the IFC to predominantly respond to these loads, thus minimizing mutual influence with the IPC. Post-filtering, the three blade root flap moments \tilde{M}_{ybi} are transformed into the fixed coordinate system via a multiplication with $2/3V_{\Psi}^T$, with the resulting moments \tilde{M}_c and \tilde{M}_s . These are both scaled with k_m to $\hat{\tilde{M}}_c$ and $\hat{\tilde{M}}_s$. Initially, two proportional controllers are used, with the manually tuned proportional parameter used as a starting point for the optimization of PID controller parameters. The transformed control outputs are then converted back for flap angle adjustments, with flap actuators modeled for a more rapid response than the pitch actuators, aiding in 2P load reduction. The TEF actuator is modeled as a first order transfer function with time constant $\tau_{\eta} = 0.05$, with the angle limited from -10° to 10° , and the rate limited from $-20^\circ/\text{s}$ to $20^\circ/\text{s}$.

4. Controller Parameter Optimization

The presented PID design is a two step approach: In a first step, initial values for the integral gain of the IPC and the proportional gain of the IFC are found via a grid search. Following this, the six AALC PID parameters are optimized with the Nelder-Mead simplex algorithm implemented in MATLAB's *fminsearch.m* to reduce the blade DEL. Both for the manual controller tuning as well as for the optimization the quality of an AALC controller are quantified via the decrease in blade root DEL. The cost function J to be minimized by the AALC is the maximum of the DEL of the three blades:

$$J = \min(\max(\text{DEL}_{\text{Bli,AALC}}/\text{DEL}_{\text{Bli,Ref}})), \quad i \in 1, 2, 3 \quad (3)$$

with $\text{DEL}_{\text{Bli,AALC}}$ derived from the blade flapwise root DEL accumulated over a simulation run with active AALC normalized by $\text{DEL}_{\text{Bli,Ref}}$ with only the baseline controller active. To evaluate and quantify the impact of an AALC controller's performance, four additional criteria are calculated: The tower DELs derived from the bending moments at the base and top of the tower, the mean and standard deviation of the generated power and the additional power requirements of the actuator due to individual pitch control. The evaluation criteria can be summarized as follows:

- **Blade $C_{\text{Bl}} = J$ and tower DEL C_{Twr} :** Reducing the blade DEL is the main incentive for using IPC to decrease the PSD at 1P. Load reductions at the 1P frequency does not influence the tower DEL, while decreasing the PSD at the 2P frequency via the flaps does also decrease the tower DEL.
- **Power mean $C_{\bar{P}}$ and standard deviation $C_{\delta P}$:** The power criteria were not included in the optimization. As the annual energy production cannot suffer from AALC, the generated power was compared for all test cases above 16 m/s and it was found that the power production loss and variance increase are negligible.
- **Actuator power C_{Act} :** This is the only criterion for which an increase is unavoidable, due to the additional, unavoidable movement of the blade that the IPC controller requires.

For evaluating the quality of the controller, the DEL at the tower base and top are also considered as

$$C_{\text{Twr},j} = \text{mean}(\text{DEL}_{\text{Twr},j,\text{AALC}})/\text{mean}(\text{DEL}_{\text{Twr},j,\text{Ref}}), \quad i \in \text{X,Y,Z}, \quad j \in \text{B,T} \quad (4)$$

with the tower base and top DEL due to fore-aft movements DEL_{TwrX} , side-wards movements DEL_{TwrY} , and torque movements DEL_{TwrZ} . Similarly, the power criterion are included as

$$C_{\bar{P}} = \bar{P}_{\text{Gen,AALC}}/\bar{P}_{\text{Gen,Ref}}, \quad C_{\delta P} = \delta P_{\text{Gen,AALC}}/\delta P_{\text{Gen,Ref}} \quad (5)$$

and the actuator power criterion as

$$C_{\text{Act}} = P_{\text{Act,AALC}}/P_{\text{Act,Ref}}. \quad (6)$$

An optimization data set with wind of turbulence class A was created to optimize the PID parameters for each wind speed separately, with the AALC's effect analyzed via the incorporation of five wind speeds in region II, from 4 m/s to 11 m/s, and nine different wind speeds in region III, ranging from 12 m/s to 25 m/s. Two verification sets were created for the 14 different wind speeds, one set with turbulence class A with a different seed and one with turbulence class B. The vertical wind speed distribution is modeled with a power law wind profile to represent wind shear, using an exponent of 0.2. All wind fields are available in the git repository [19], which also includes the code to reproduce all results presented in this paper.

5. Results

This section discusses both open loop results, obtained with the simulation set-up depicted in Figure 4, as well as closed loop results, simulated with the control loop from Figure 5. Figure 6 and Figure 7 show the steady state values, at three different TEF angles, of power P_{gen} , rotor speed n_{rot} , rotor thrust T_{rot} , and blade pitch angle β_0 for all 14 wind speeds. Simulations at constant wind speeds are run for 660s to confirm the validity of the TEF model. Data from the initial 60s are excluded to avoid non-physical initialization artifacts and the mean values are calculated for each wind speed. The simulated power with and without TEF deflections

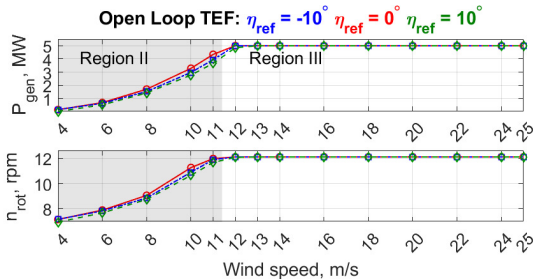


Figure 6. TEF open-loop validation of power and rotor speed, TEF deflection at -10° (blue), 0° (red), and 10° (green).

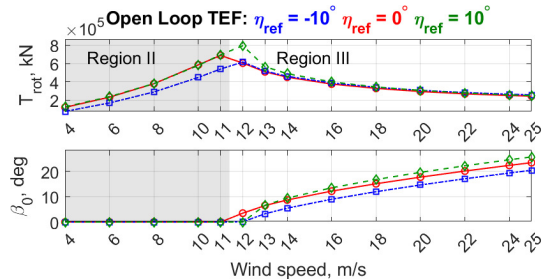


Figure 7. TEF open-loop validation of rotor thrust and blade pitch, TEF deflection at -10° (blue), 0° (red), and 10° (green).

shows the expected power characteristic curve of a wind turbine: In region II, both positive and negative flap deflection reduce power P_{gen} due to decreased aerodynamic efficiency, unlike in region III, where the same power output is observed, as the power controller controls the pitch angle once rated wind speed is reached. Adjusting the pitch changes the aerodynamic forces. The control system can therefore maintain nominal power. This also reflects on the rotor speed n_{rot} , depicted in the second plot, which is slightly lower in region II but unchanged in region III. The thrust T_{rot} in region II is decreased by a negative flap angle, while the influence of a positive flap angle on the thrust is negligible: The thrust cannot be increased beyond the neutral flap position due to the limited wind power, which necessarily limits the amount of energy converted into rotational energy. This leads to a dynamic equilibrium where, despite positive flap deflection, the thrust forces remain at levels equivalent to those at the neutral flap position. The second plot in Figure 7 shows the blade pitch β_0 , which is lower for a negative and higher for a positive TEF angle, corresponding to the lower and higher thrust force. Figure 8 shows the power spectral density (PSD) of the blade root bending moment in closed-loop for the first verification data set with a mean wind speed of 16 m/s. IPC (blue line) and IFC (green line) reduce the PSD of the

1P and 2P loads, respectively, compared to the baseline (black line). These PSDs are obtained with the initially used AALC parameters with the original setting of a purely integral IPC and a purely proportional IFC feedback, both set to values of one. In a first optimization step, only the two controller parameters $K_{I,IPC}$ and $K_{P,IFC}$ are optimized. In a second step, the four additional parameters of the two PID controllers are optimized as well, resulting in an IPC PI controller, with $K_{P,IPC} = 0.354$ and $K_{I,IPC} = 1.194$ and an IFC P controller with $K_{P,IPC} = 0.631$. Figure 9 demonstrates that considerable improvement with respect to the baseline controller is possible using the suggested AALC design: The combined IPC-IFC control with the original setting of a purely integral IPC and proportional IFC feedback reduces the PSD at 1P by 97.9%, and at 2P by 79.9%. Adding and optimizing additional parameters improves the AALC's effect only slightly further, with a reduction at 1P of 98.5% and 2P of 69.8% with respect to the baseline. With regard to the selected starting values of the AALC, this is a further reduction at 1P of 27.5%, but an increase at 2P of 50.1%. The cost function of the two controllers is at $J = 0.880$ for the initial controller and at $J = 0.877$ for the optimized one. From this study, it seems unlikely that a parameter optimization of the suggested, carefully designed controller can decrease the blade damage equivalent loads considerably. Further investigations might be made with respect to how much improvement is achievable with a more sophisticated MIMO controller. Apart from the blade root flapwise moment, the influence of the obtained controller parameters is compared with respect to the evaluation criteria provided in section 4. Table 1 contains the five evaluation criteria to quantify the effect of the AALC as given in equations (4) to (6): Blade and tower DEL, mean of generated power \bar{P}_{Gen} , its standard deviation δP_{Gen} , and actuator power P_{Act} . The mean of the five criteria for all five simulations covering the part of region III above 16 m/s is normalized through simulations without AALC with the same wind test cases. Blade DEL decrease by 20% and 22%. Tower bottom DEL and top DEL are decreased by between 1% and 3% for the verification sets. The evaluation of the power criteria confirms that the AALC leads only to negligible changes in both power mean and variance. The additional rotational movement of the blade demanded by IPC is the only criterion leading to an unavoidable increase. Future research will focus on finding a reasonable balance between reducing DEL and managing the unavoidable increase in pitch actuator activity. This might include using additional optimization criteria or explicit constraints, either for the presented controller or for MIMO designs, as well as investigating alternative AALC techniques, see e.g. [20] for sectional lift control.

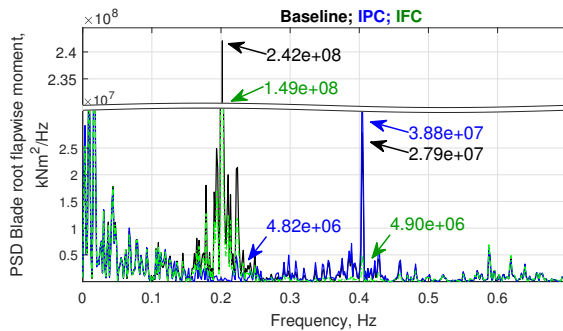


Figure 8. PSD at 16 m/s, Baseline (black), IPC (blue), and IFC (green).

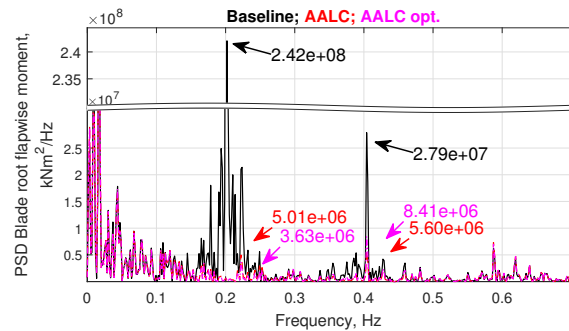


Figure 9. PSD at 16 m/s, Baseline, AALC (red), AALC optimized (pink).

Table 1. Mean evaluation criteria wind test cases from 16 m/s to 25 m/s

Data set	Turb. class	C_{Bl}	$C_{Twr,B}$	$C_{Twr,T}$	$C_{\bar{P}}$	$C_{\delta P}$	C_{Act}
Optim.	A	0.77	0.98	0.96	1.00	1.00	2.94
Verif. 1	A	0.80	0.99	0.98	1.00	1.01	2.84
Verif. 2	B	0.78	0.99	0.97	1.00	1.01	3.09

6. Summary

An active aerodynamic load control system integrating individual blade pitch and trailing-edge flap control was added to the OpenFAST model of the NREL 5MW wind turbine to minimize blade root moments. This model, extended to include additional aerodynamic coefficients for deflected trailing-edge flaps, was tested in Simulink with the FASTTool power controller. A plausibility study demonstrated that blade aerodynamic efficiency decreases with flap deflection, but that efficiency losses at high wind speeds are compensated by the power controller. A SISO multi-loop controller with inverse notch filters was developed for blade load reduction, optimized via the Nelder-Mead simplex algorithm, addressing 1P loads through individual pitch control and 2P loads through trailing-edge flap control. The pitch control notably lowered these moments, and flap control further reduced them while also lessening tower base moments.

References

- [1] Hoffmann A and Weiß F 2016 *Journal of Physics: Conference Series* vol 753 (IOP Publishing) p 052020
- [2] Selvam K, Kanev S, van Wingerden J W, van Engelen T and Verhaegen M 2009 *International Journal of Robust and Nonlinear Control: IFAC-Affiliated Journal* **19** 72–91
- [3] Petrović V, Jelavić M and Baotić M 2021 *Wind Energy* **24** 54–68
- [4] Ossmann D, Seiler P, Milliren C and Danker A 2021 *Renewable Energy* **170** 1245–1256
- [5] Bossanyi E, Savini B, Iribas M, Hau M, Fischer B, Schlipf D, van Engelen T, Rossetti M and Carcangiu C 2012 *Wind Energy* **15** 119–145
- [6] Zhang M, Tan B and Xu J 2015 *Renewable Energy* **77** 217–226
- [7] Bergami L and Hansen M H 2017 *Wind Energy* **20** 431–447
- [8] Wilson D G, Berg D E, Resor B R, Barone M F and Berg J C 2009 Combined Individual Pitch Control and Active Aerodynamic Load Controller Investigation for the 5MW UPWIND Turbine. Tech. rep. Sandia National Lab.(SNL-NM), Albuquerque, NM (United States)
- [9] Henriksen L C, Bergami L and Andersen P B 2013 *European Wind Energy Conference & Exhibition 2013* (European Wind Energy Association (EWEA))
- [10] He K, Qi L, Zheng L and Chen Y 2018 *Energies* **11** 2519
- [11] Osterwinter B 2023 Kombinierte individuelle Blatt- und Hinterkantenklappenregelung zur Lastminimierung bei Windkraftanlagen Tech. rep. German Aerospace Center (DLR), Brunswick, Germany
- [12] National Renewable Energy Laboratory (NREL) 2023 OpenFAST <https://openfast.readthedocs.io/en/main/>
- [13] Jonkman J, Butterfield S, Musial W and Scott G 2009 Definition of a 5MW Reference Wind Turbine for Offshore System Development Tech. rep. National Renewable Energy Lab.(NREL), Golden, CO (United States)
- [14] Drela M 1989 *Low Reynolds Number Aerodynamics: Proceedings of the Conference Notre Dame, Indiana, USA, 5–7 June 1989* (Springer) pp 1–12
- [15] Gasch R and Tvele J 2011 *Windkraftanlagen: Grundlagen, Entwurf, Planung und Betrieb*
- [16] Mulders S, Zaaier M, Bos R and van Wingerden J 2020 *Journal of Physics: Conference Series* vol 1452
- [17] Ossmann D, Theis J and Seiler P 2017 *Wind Energy* **20** 1771–1786
- [18] Dittmer A, Sharan B and Werner H 2021 *2021 European Control Conference (ECC)* (IEEE) pp 1544–1549
- [19] Dittmer A and Osterwinter B 2024 Code for paper 'combined ipc and tefc for load reduction of wind turbines' <https://github.com/antjedittmer/Combined-IPC-TEFC-for-Load-Reduction-of-Wind-Turbines>
- [20] Gupta A, Rotea M A, Chetan M, Sakib M S and Griffith D T 2022 *Journal of Physics: Conference Series* vol 2265 (IOP Publishing) p 032093